A Systematic CFD-Based Examination of Rotor-Rotor Separation Effects on Interactional Aerodynamics for Large eVTOL Aircraft

Richard Healy
PhD Student

Matthew Misiorwoski
PhD Student

Farhan Gandhi
Redfern Professor

Center for Mobility with Vertical Lift (MOVE)
Rensselaer Polytechnic Institute, New York, USA

ABSTRACT

This study systematically investigates the aerodynamic interactions of a two-rotor system with a front rotor and an aft rotor aligned with the direction of flow. The rotors are 5.5 ft diameter fixed-pitch rotors operating at around 12 lb/ft^2 disk loading, representative of large eVTOL aircraft. Fluid flow is simulated using the commercial Navier-Stokes solver, AcuSolve, with a Detached Eddy Simulation (DES) model. Simulations were performed at 40 kts edgewise flight for 9 cases corresponding to three values of longitudinal hub-hub separation ($2.5R$, $3R$, $3.5R$) and three values of vertical offset (0, $0.25R$, $0.5R$). Aft rotor performance was compared to an isolated rotor operating in the same conditions in order to quantify the effects of rotor-rotor interaction. For the cases where the aft rotor is closest to the front rotor ($2.5R$ longitudinal offset, zero vertical offset), the aft rotor produced 8.4% less thrust, and required 13.4% higher torque than a rotor in isolation. When vertical rotor separation was increased, interactional aerodynamic effects decreased. For a $2.5R$ longitudinal offset, increasing the vertical offset to $0.5R$ decreased the lift deficit to 4.6% and the torque penalty to 6.8%. Increasing the longitudinal offset to $3.5R$ (while keeping the vertical offset at zero) also reduced interactional aerodynamic effects, but reductions in lift deficit and torque penalty were smaller than those observed with $0.5R$ vertical offset.

INTRODUCTION

Small multi-rotor drones are an emerging technology that have to date been mostly used by hobbyists and aerial photographers/videographers. Recently, electric multicopters have been more seriously considered for urban transportation (the Uber Elevate vision), commercial (package delivery, inspection), and military/law-enforcement applications, where aircraft performance is increasingly important. The current batteries powering most of these multi-copters exhibit limitingly low energy density relative to hydrocarbon fuels used by larger convectional VTOL aircraft. With this shortcoming, it is especially important to maximize their aerodynamic performance in order to realize practical payload capacity, endurance and range. One area that requires particular attention is the understanding of the interactional aerodynamic effects of rotors operating in close proximity, and its impact on performance.

Given the highly complex nature of the interactional aerodynamics of multi-rotor aircraft, there have been a number of recent studies using high-fidelity Computational Fluid Dynamics (CFD) simulations. Researchers at the NASA Advanced Supercomputing Division used CFD to simulate both large as well as small-scale quadcopters. Yoon et al. (Refs. 1, 2) investigated the effects of turbulence modeling and rotor separation for an XV-15 derivative quadcopter design in hover

and determined that decreasing the separation between rotors reduces the thrust generated by up to 4%. Yoon et al. also simulated the small scale Straight Up Imaging (SUI) Endurance quad-copter (Ref. 3) and determined that at 10 m/s cruise, the rear rotors produced 28% less thrust than they would if operating in isolation. Studies by Tanabe et al. (Ref. 4) indicated a significant rotor-to-rotor interference effect in hover when the clearance between adjacent rotor blade tips reduced to less than half of the rotor radius. More recent computational studies by NASA Ames include the work of Diaz and Yoon (Refs. 5, 6), which looked at over-/under-mounting rotors on a quad-copter, finding that a vertical offset between the front and rear rotors decreased interference. In (Ref. 7), Misiorowski, Gandhi and Oberai used CFD to examine a quad-copter in cruise operating in both "plus" and "cross" configurations, and provided physical insight into the difference in interactional aerodynamics between the two operational configurations.

Whereas the studies above have simulated specific multi-rotor configurations, the present research focuses on a systematic examination of rotor-rotor separation on interactional aerodynamic effects. With two rotors aligned in the direction of flight, the longitudinal spacing of the aft rotor is parametrically varied relative to the front rotor, and the vertical offset is varied as well. The CFD simulations use the commercial Navier-Stokes solver AcuSuolve (similar to Ref. 7), but consider larger rotor size and higher disk loading which is more representative of vehicles of interest in the urban air mobility and human transport context. Moreover, this study looks to identify the aerodynamic mechanisms that cause the change

in rotor-rotor interaction.

METHOD

The rotor used in the current study is a modified $5\frac{1}{2}$ foot diameter two-bladed Whirlwind propeller (Ref. 8). The blade chord distribution is shown in Fig. 1. The original Whirlwind propeller is untwisted, fixed pitch (no cyclic pitch) and intended for axial flow applications. Most eVTOL designs utilize fixed pitch rotors, so an appropriate root pitch value and twist are first selected for this study.
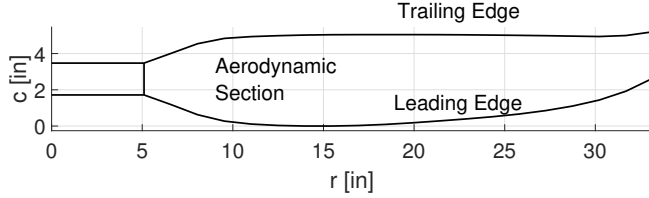

Fig. 1. Blade planform (chord distribution)

The Rensselaer Multirotor Analysis Code (RMAC) (Ref. 9), based on blade element theory (BET) with 3x4 finite state Peters-He inflow representation is used to evaluate the performance associated with possible modifications to the Whirlwind propeller. For a sweep of tip pitch and twist rates, the rotor speed is trimmed in hover to match a pre-selected target disk loading representative of a large eVTOL aircraft ($12 lb/ft^2$ (Ref. 10)). Figure 2 shows the corresponding tip mach number for the trimmed rotor speed at each tip pitch and twist rate, and the associated power requirement. A tip pitch of $12°$ and twist rate of $-12°/R$ is found to be a good balance between low tip mach number ($M = 0.56$) and low power. To maintain a hover disk loading of $12\ lb/ft^2$, a blade rotational speed of 2170 RPM is required.

CFD simulations are carried at a forward speed of 40 kts, with the majority of the simulations being for a two-rotor unit comprising of a front rotor and an aft rotor set at various separation distances relative to the front rotor, as shown in Fig. 3. The two-rotor unit is set at a nose-level pitch attitude relative to the free-stream as many large eVTOL designs utilize a dedicated propeller for propulsion. The aft rotor of the two rotor unit is set at 2.5, 3 and 3.5 rotor radii longitudinal separation (hub to hub) from the front rotor, in the free-stream direction. Simulations include the aft rotor in-plane, as well as at vertical offsets of 0.25 and 0.5 rotor radii above the front rotor. All of the simulated two-rotor configuration cases are shown in Fig. 3 (nine cases in all).

CFD simulations are conducted using the commercial Navier-Stokes solver AcuSolve which uses a stabilized 2nd order upwind finite element method. AcuSolve simulation results for an SUI Endurance rotor were previously shown to compare well against experiment in Ref. 7. For a two-rotor unit, the computational domain is shown in Fig. 4 comprising of a rectangular prism with far-field boundary conditions on the front
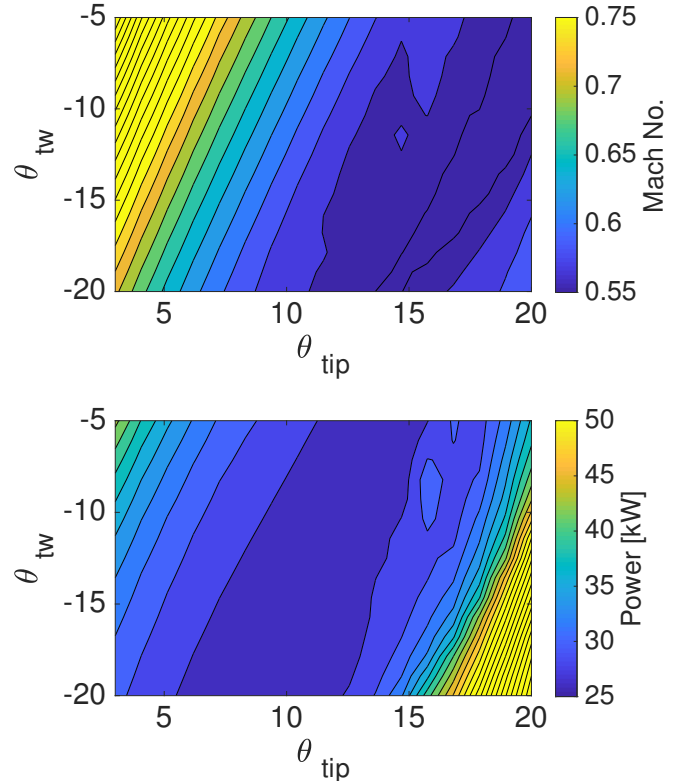

Fig. 2. Tip mach number and power requirement for variation in twist rate and pitch setting
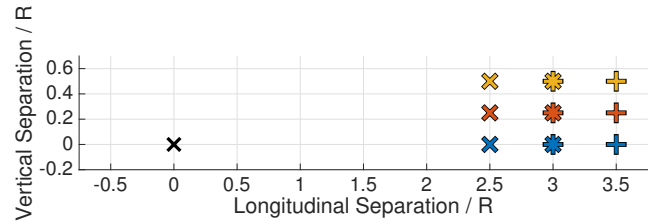

Fig. 3. Aft-rotor hub position relative to front rotor

and top surfaces set to the freestream velocity. The sides, bottom and rear of the computational domain are set to outflow with backflow conditions enabled, which allows for flow in either direction across the boundary with zero pressure offset. All boundaries of the computational domain are at least 25 rotor radii away from the center of the aircraft in all directions. As indicated in Fig. 4, the computational domain consists of two rotating volumes (for the two-rotor unit) where the mesh inside the volume rotates along with the rotor geometry. Each rotating volume is a cylinder with radius 1.06 rotor radii. The height of the cylinder extends two tip chord lengths above and below the rotor plane. Each rotating volume is bounded by a sliding mesh interface which passes information into and out of the non-rotating volume that comprises the remainder of the computational domain.

The domain was discretized using a mesh comprised entirely of unstructured tetrahedral elements. Within both rotating vol-

Table 1. Average rotor thrust for isolated rotors with different mesh parameters

Mesh	Integrated Thrust [N]	Thrust % Difference from Baseline	Torque [Nm]	Torque % Difference from Baseline
Baseline	1174.1	-	74.8	-
4x Boundary Layer	1172.2	0.16	74.6	0.27
2x LE/TE Refinement	1175.8	0.14	75.1	0.4
2x Chordwise Elements	1160.1	1.2	73.6	1.6
2x Wake Refinement	1186.2	1.0	73.67	2.4
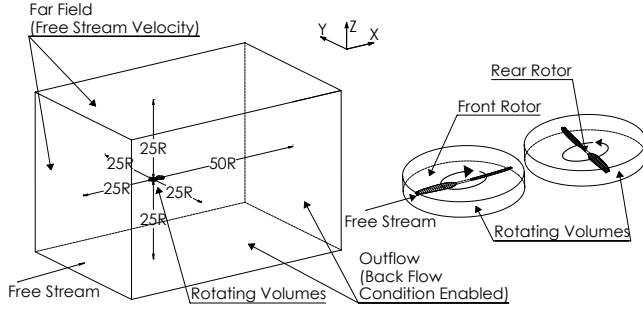
Fig. 4. Diagram of the computational domain

Fig. 5. Cross-section of wake mesh refinement

umes, the blade surface mesh was set to ensure 200 elements around the airfoil. The elements on the blade were refined by a factor of 10x near the leading (0-10% chord) and trailing edge (90-100% chord), compared to the elements along the remainder of the chord. The boundary layer in the wall normal direction is highly resolved, with the first element height set to ensure $y+ < 1$. A refinement region, with element size prescribed as $\frac{1}{2}$ tip chord is established for the off-body area around the rotors, and extends 0.3R above the rotor plane, and 1.5R below (Fig. 5), with the mesh refinement below the rotor plane skewed towards the rear to better capture the rotor wakes as they convect downstream. The entire computational domain is comprised of 10 million grid points, with 4 million in each rotating volume, and 2 million in the nonrotating volume. A mesh refinement study was performed in which the surface mesh size, edge refinement, boundary layer, and wake refinement were doubled independently. The results of the refinement study are shown in table 1. For an isolated rotor in 40 knot edgewise flight, the thrust and torque changed by less than 1.5% and 2.5% respectively when compared to the original mesh (which is used for simulations in this study).

A detached eddy simulation (DES) is used with the Spalart-Allmaras (SA) turbulence model for all cases. All simulations were run initially using time steps corresponding to $10°$ of rotation for several revolutions to reduce computational cost of the rotor wake development. Each simulation was then restarted for additional revolutions at $1°$ time steps until convergence was achieved. The initial $10°$ time steps are possible without causing numerical divergence due to the stability afforded by the Streamline Upwind Petrov-Galerkin (SUPG) stabilized finite element method and Generalized α implicit
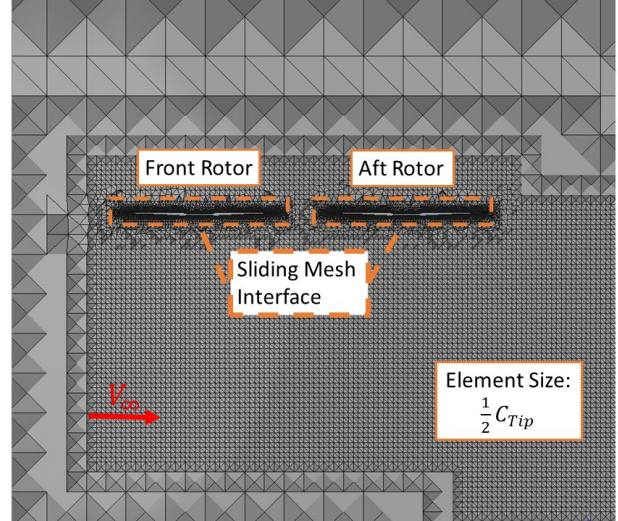
time integration method. The latter method was designed to suppress high frequency distrubances and allow solution stability with Courant-Friedrichs-Lewy (CFL) number greater than 1 (Refs. 11, 12). All runs were performed on 512 2.6 GHz Intel Xeon E5 -2650 processors, part of the Center for Computational Innovations (CCI) at Rensselaer Polytechnic Institute.

RESULTS

Isolated Rotor Aerodynamics

Forward flight simulations were conducted to first evaluate and analyze thrust production of an isolated rotor. Figure 6 shows the sectional thrust coefficient (dC_T/dx) for a counter clockwise spinning isolated rotor in 40 knot edgewise flow at 2170 RPM. This represents the operational state of the aft rotor in the system described above without the presence of a front rotor. A region of higher thrust can be seen on the advancing side of the rotor around $\psi = 110°$. This feature is consistent with that seen in (Ref. 7), and is caused by higher dynamic pressure on the advancing side of the rotor, as well as longitudinal inflow variation (Ref. 13).
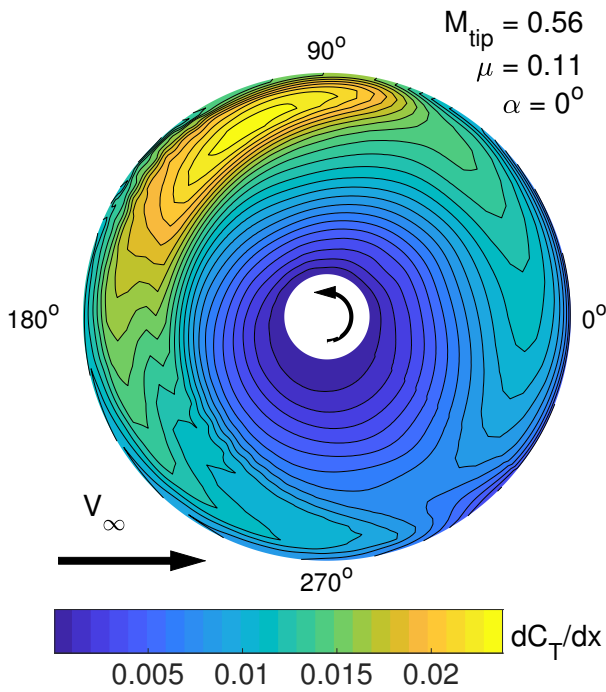
Fig. 6. Sectional thrust coefficient, dCt/dx, for isolated rotor

Interactional Aerodynamics in a Two Rotor System

With the thrust properties of an isolated rotor established, the thrust production of a two rotor system is investigated. Figure 7 shows the sectional thrust coefficient (dC_T/dx) for a two rotor system with 2.5R longitudinal separation and no vertical separation. Compared to the isolated counter-clockwise spinning rotor (6), the aft rotor of this configuration exhibits a smaller area of high thrust on its advancing side. Additionally, the area of high thrust moves back from $\psi = 110°$ to $\psi = 90°$. The front rotor (also set at zero pitch attitude and spinning at 2170 RPM) exhibits no notable difference from an isolated clockwise rotor, indicating the presence of the aft rotor has no notable effect on the front rotor.
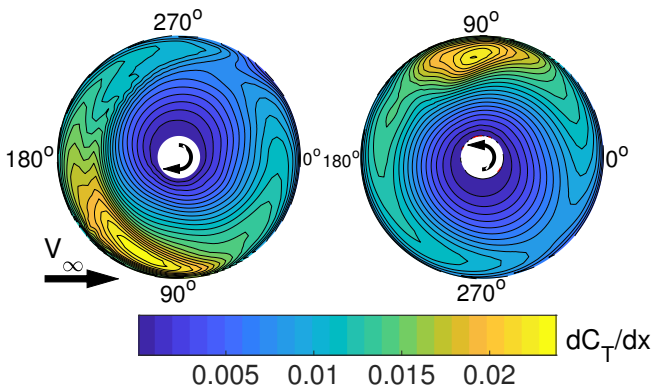

Fig. 7. Sectional thrust coefficient, dCt/dx, for 2.5 rotor radii separation

Front Rotor Wake Aerodynamics

The aerodynamics of a front rotor in isolation are investigated in order to gain insight on how the front rotor interacts with the aft rotor. Figure 8 shows the Q-criterion for an isolated rotor colored by x-vorticity. The region occupied by an aft rotor with 2.5R longitudinal separation and no vertical separation is also shown, colored by z induced velocity. Inside the wake, the vortex rollup from both the front rotor's advancing and retreating sides induces downwash, indicated by the blue region on the location of the aft rotor disk (no aft rotor actually present in the simulation). Downwash is stronger on the front of the rotor disk, and grows weaker towards the back of the rotor disk as the front rotor wake convects downwards. However, outside the wake, the vortex rollup induces upwash. The wake from the front rotor is observed to tilt toward its advancing side as it convects downstream. As a result, the retreating side of the aft rotor sees only downwash, but the advancing side of the aft rotor (which lies outside the front rotor wake) sees front rotor wake induced upwash.
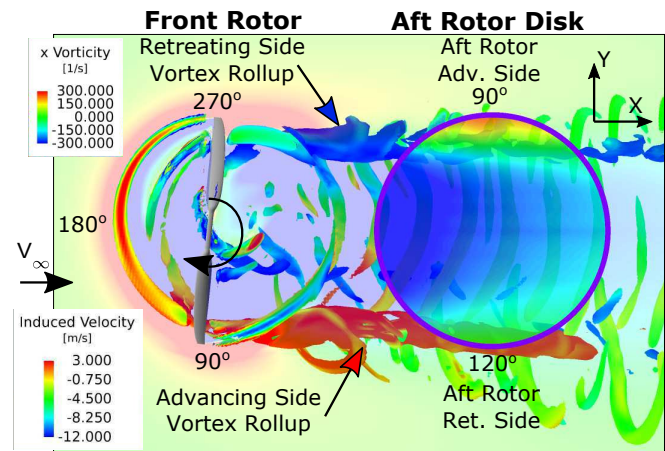

Fig. 8. Q-Criterion (20,000) of isolated rotor wake colored by vorticity in the freestream direction and induced velocity in the region of the aft rotor disk

Figure 9 shows the Q-criterion for an isolated clockwise spinning rotor, colored by x-vorticity as viewed from the side. The red super tip vortex from the advancing side convects faster downward than that the blue super tip vortex retreating side due to the higher lift generation and higher downwash on the advancing side. By the time the wake reaches the aft rotor disk, the advancing side super tip vortex, albeit stronger, has convected below further down than the retreating side super tip vortex. Less downwash is induced on the retreating side of the aft rotor disk (as seen in figure 8) due to the relatively lower position of the advancing side super tip vortex.
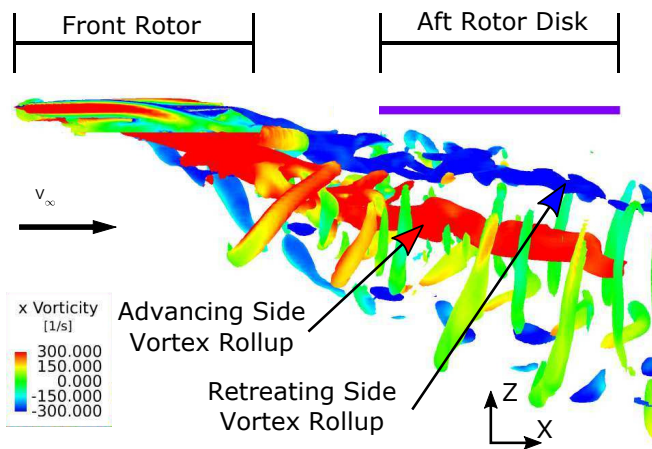
4

Fig. 9. Q-Criterion (15,000) of isolated rotor wake colored by vorticity in the freestream direction

The presence of downwash and upwash on the aft rotor disk discussed above are what cause the change in its rotor thrust relative to an isolated rotor operating at the same conditions (forward speed, pitch attitude and RPM). Figure 10 shows the difference in sectional thrust coefficient between an isolated aft rotor and an aft rotor with 2.5R longitudinal separation. Downwash seen in Figure 8 causes a decrease in thrust near the front of the rotor. Additional downwash on a blade element reduces the effective angle of attack by increasing the local inflow angle. The reduction in angle of attack on the blade element reduces local blade lift. A region of increased thrust is also seen outboard on the advancing side due to upwash from the front rotor's retreating side vortex rollup.
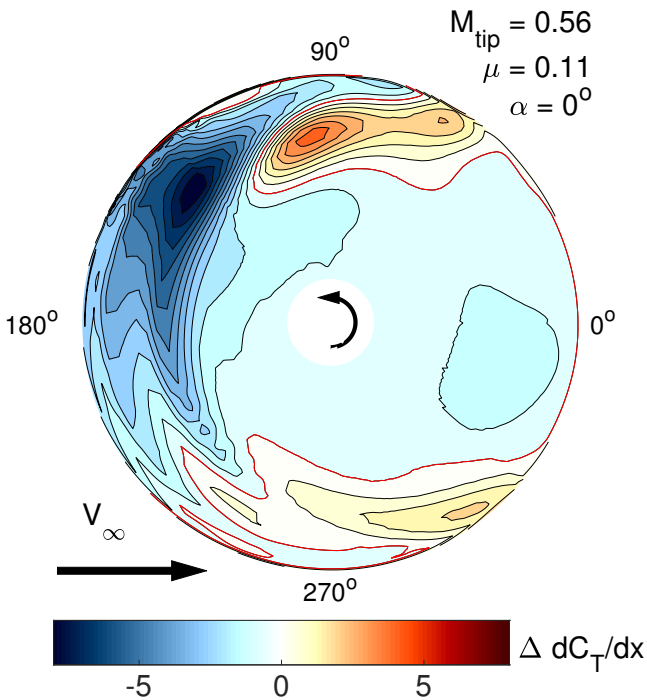

Fig. 10. Sectional thrust coefficient difference, $\Delta dC_T/dx$ (2.5R longitudinal separation subtracting isolated)

The difference in rotor thrust observed between an aft rotor in a two rotor system and an isolated rotor is similar to that seen in (Ref. 7). In both cases, the aft rotor experiences a loss in lift on the front of the rotor disk. Additionally, a region of increased thrust is seen at about $\psi = 90°$ due to upwash from the front rotor's retreating side vortex rollup.

Impact of Rotor Spacing on Thrust

The velocity induced by the front rotor on the aft rotor disk depends on the position of the aft rotor disk. Figure 11 shows the velocity induced by an isolated front rotor over a vertical plane cutting through the front of the aft rotor disk situated at 2.5R longitudinal separation and three different vertical positions. A region of blue downwash can be seen over this vertical plane cutting through the forward section of the aft rotor locations (no aft rotor actually present in this simulation). As the aft rotor is moved up from position A (in plane with the front rotor) to positions B and C (0.25R and 0.5R vertical offset respectively), the downwash in the rotor plane decreases. The figure also shows the position of the front rotor's advancing and retreating side tip vortices. The retreating side tip vortex, which generates upwash and lift increment on the aft rotor's advancing side (Figs. 8 and 10) is further from the aft rotor as it moves up to positions B and C. Thus, the advancing side upwash and lift increment can be expected to weaken.
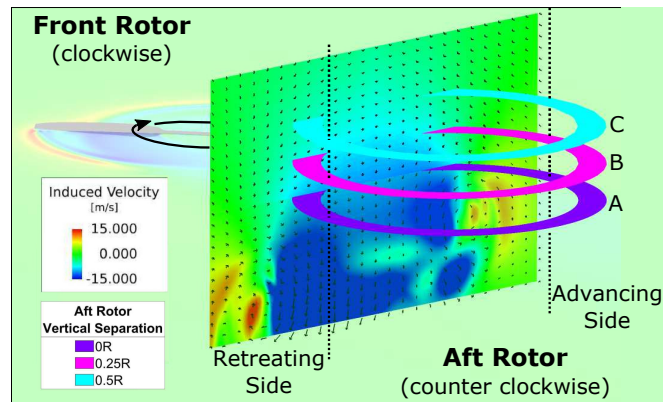

Fig. 11. Velocity induced by the front rotor on the area occupied by the aft rotor at 2.5R longitudinal separation

Figure 12 shows the difference in sectional thrust coefficient (thrust coefficient of aft rotor minus that of an isolated rotor at the same operating conditions) for aft rotors located at 2.5R longitudinal separation and different vertical separations. The velocity induced by an isolated front rotor at the corresponding location occupied by each aft rotor is also presented. As the aft rotor is moved up, out of the plane of the front rotor, the interactional aerodynamic effects are observed to diminish. Both downwash over the front section of the aft rotor disk and upwash on the outboard sections of the advancing blade decrease in magnitude. At 0.25R vertical separation, the peak loss in lift reduces in magnitude when compared to no vertical separation. Similarly, the peak increase in lift seen on
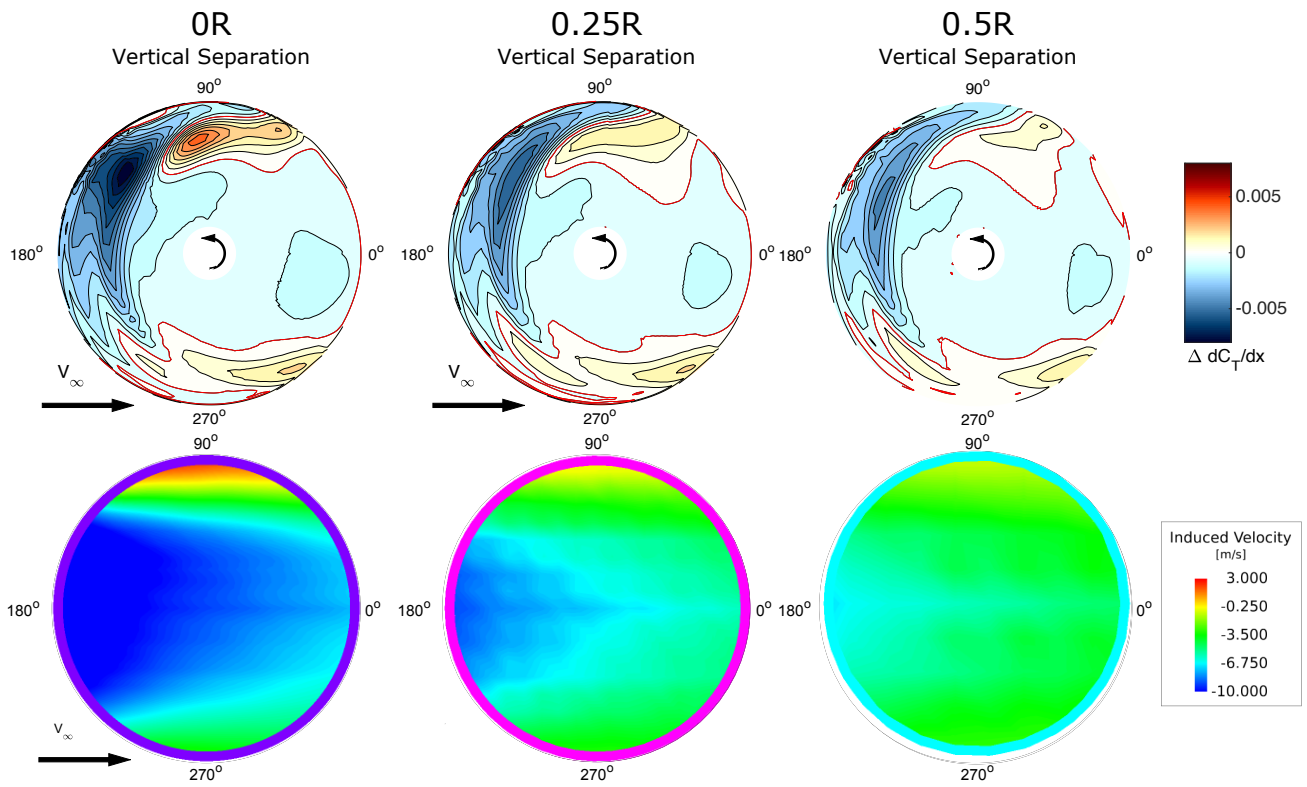
Fig. 12. Difference in sectional thrust coefficient and induced velocity experienced from the front rotor for aft rotors with different vertical separations and 2.5R longitudinal separation
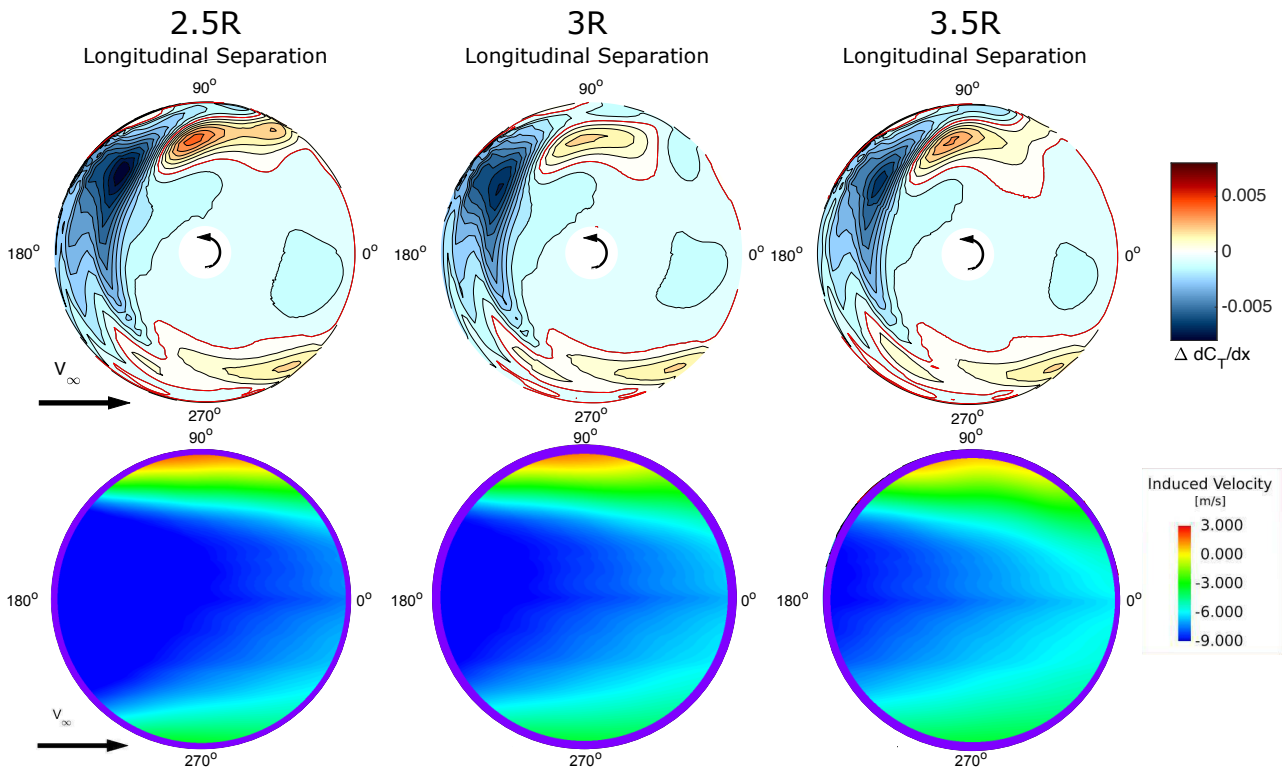

Fig. 13. Difference in sectional thrust coefficient for aft rotors with different longitudinal separations and no vertical separation

the aft rotor's advancing side is also lower at 0.25R vertical separation. At 0.5R vertical, the region of reduced lift is even smaller than that seen at 0.25R vertical separation. However, the change in peak lift reduction between 0R and 0.25R is greater than that seen between 0.25R and 0.5R. The increase in lift observed from vortex rollup on the aft rotor's advancing side also reduced as the aft rotor is moved up, away from the front rotor's retreating side vortex.

Figure 13 shows the difference in sectional thrust coefficient (thrust coefficient of aft rotor minus that of an isolated rotor at the same operating conditions), subtracting the isolated rotor from aft rotors at different longitudinal separations, and no vertical separation. Again, the induced velocity from the front rotor at the location occupied by each aft rotor is also shown. As longitudinal spacing increases, the decrease in thrust observed on the front of the rotor disk reduces in magnitude. Additionally, the increase in thrust seen on the advancing side of the aft rotor decreases in magnitude, as well. These observations are corroborated by the decrease in downwash at the front and upwash in the vicinity of the advancing blade tip as longitudinal spacing is increased.

Figure 14 shows the relative difference in total rotor thrust between an aft rotor for the separation cases considered and an isolated rotor. An aft rotor with small longitudinal spacing and no vertical spacing (2.5R; 0R) experiences the largest loss in lift when in the presence of a front rotor (−8.4%). Keeping longitudinal spacing constant, as vertical spacing is increased, the aft rotor lift deficit reduces. At close longitudinal separation (2.5R), the change observed when moving from no vertical offset (8.4% lift deficit) to 0.25R (5.6% lift deficit) is greater that that seen when moving from 0.25R to 0.5R (4.6% lift deficit). This trend holds for all longitudinal separations, where the biggest improvement is gained with the initial induction of vertical offset, and subsequent offsets provide smaller improvement.
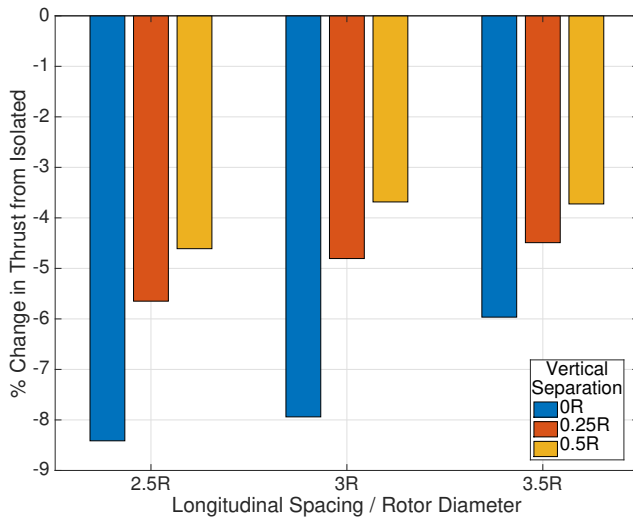
Increasing longitudinal separation also reduces the negative impact of a front rotor. Keeping the aft rotor in-plane with the front rotor, an increase from 2.5R (8.4% lift deficit) to 3R (7.9% lift deficit) longitudinal spacing results in a smaller change than moving from 3R to 3.5R (5.8% lift deficit). However, this trend does not hold when considering higher vertical separations. If 0.25R vertical offset is used, an increase from 2.5R (5.6% lift deficit) to 3R (4.8% lift deficit) results in a larger change than from 3R to 3.5R (−4.3%). In general, these results suggest that both longitudinal separation and vertical separation are viable methods for reducing rotor-rotor interaction in a two-rotor system; but a 0.5R vertical offset is slightly more effective than a 1R increase in longitudinal offset.

Impact of Rotor Spacing on Torque

Figure 15 shows the sectional torque coefficient for an isolated rotor with 2.5R longitudinal separation and no vertical separation. Figure 18 shows the difference in sectional torque coefficient between an isolated aft rotor and an aft rotor with 2.5R longitudinal separation. The aft rotor exhibits more drag near the front of the rotor disk due to the high downwash induced by the front rotor in this area.
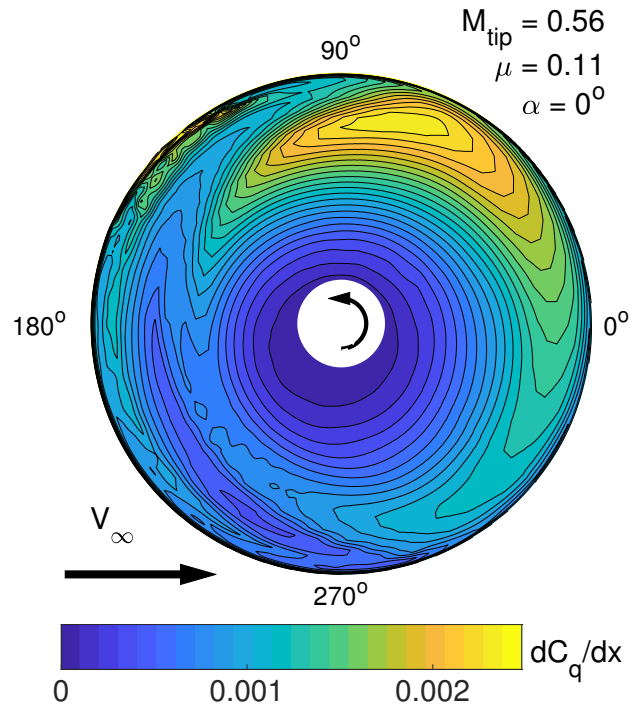

Fig. 15. Sectional torque coefficient dC_Q/dx **for isolated rotor**

Fig. 14. Relative difference in rotor thrust for isolated and aft rotors in two rotor system at different longitudinal and vertical separations

Figure 16 shows the sectional torque coefficient for aft rotors with 2.5R longitudinal separation and different vertical separations. As vertical separation is increased, the region of high drag observed on the front of the rotor disk decreases. The less intense downwash experienced by the rotors with greater vertical separation peak drag to be lower in magnitude.

Figure 17 shows the sectional torque coefficient for aft rotors with various longitudinal separations and no vertical separation. As longitudinal separation is increased, the magnitude of drag on the front of the aft rotor disk slightly decreases. As with rotor thrust, the decreased downwash experienced by aft rotors with larger longitudinal spacing reduces interactional aerodynamic effects.

Figure 19 shows the net difference in rotor torque between aft rotors in a two rotor system and an isolated rotor. The aft rotor with 2.5R longitudinal separation and no vertical separation exhibits the greatest increase in rotor torque (13.4%). As vertical separation is increased, the torque penalty reduces. At close longitudinal separation (2.5R), the improvement when going from no vertical offset (13.4% penalty) to 0.25R (9.8% penalty) is similar to that observed when progressing from 0.25R to 0.5R (6.8% penalty).
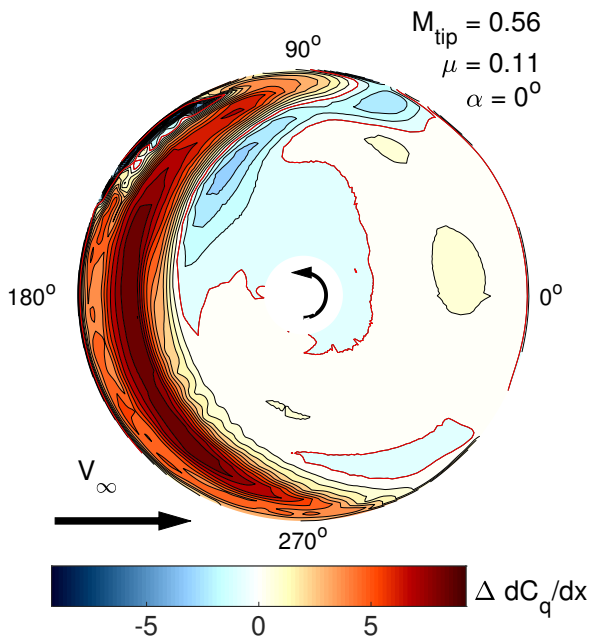
Fig. 18. Difference in sectional torque coefficient, $\Delta dC_Q/dx$ (aft rotor minus isolated rotor) for $2.5R$ longitudinal separation and no vertical separation
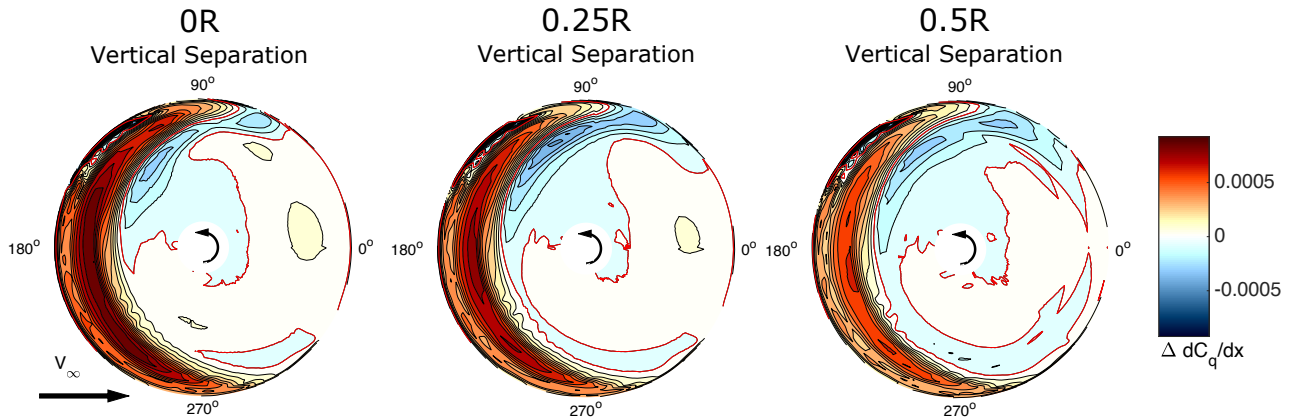

Fig. 16. Difference in sectional torque coefficient, dC_Q/dr (aft rotor minus isolated rotor) for aft rotors with $2.5R$ longitudinal separation and different vertical separations
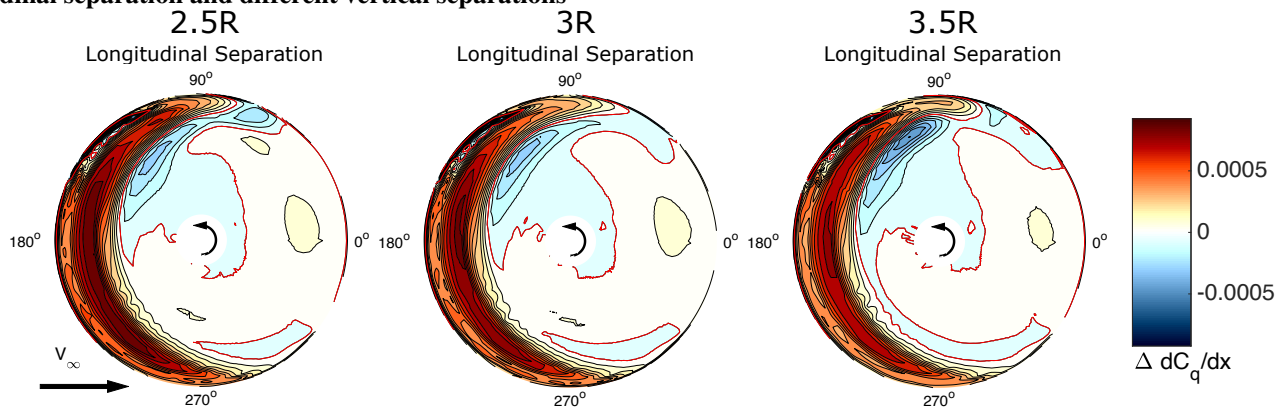

Fig. 17. Difference in sectional torque coefficient, dC_Q/dx (aft rotor minus isolated rotor) for aft rotors with various longitudinal separation and no vertical separations

8

Longitudinal separation is also seen to influence aft rotor torque. When in-plane, relatively little change is seen when going from $2.5R$ (13.4% penalty) to $3R$ (12.9% penalty). However, moving from $3R$ to $3.5R$ (10.4% penalty) is seen to provide relatively more substantial improvement. At highest vertical offset, increasing the longitudinal offset is relatively uninfluential (compare the three yellow bars on Fig. 19 for torque). Similar observation could also be made for thrust (Fig. 14).
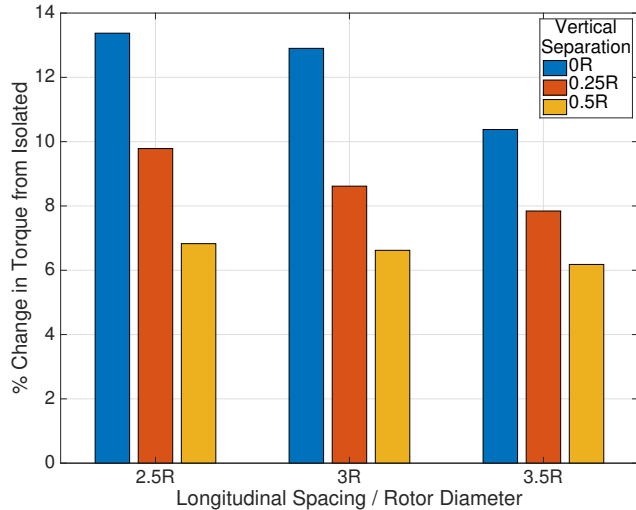

Fig. 19. Relative difference in torque for aft rotors in a two rotor system

CONCLUSIONS

This study investigates the impact of longitudinal and vertical separation on the interactional aerodynamics of a counter rotating two rotor system in edgewise flight, relevant to current large eVTOL interests. Fluid flow simulations were performed using the commercial CFD code AcuSolve, with a Detached Eddy Simulation (DES). The rotating volume around each rotor interfaces with the remainder of the computational domain using a sliding mesh. All simulations were performed for twisted $5\frac{1}{2}$ foot diameter Whirlwind propellers with $24°$ root pitch. Rotor RPM was set to target $12 lb/ft^2$ disk loading using a BET trim code. In total, 9 two rotor system simulations were performed for varying longitudinal and vertical rotor separations. In particular, 3 longitudinal separations ($2.5R, 3R, 3.5R$), and 3 vertical separations ($0R, 0.25R, 0.5R$) were considered. The thrust and torque from each simulation were compared to those for an isolated rotor operating in the same conditions. Through these simulations, the following observations were made.

1. For all simulated separation distances, the wake of the front rotor induced downwash on the aft rotor disk. More downwash was observed on the front of the aft rotor disk than on the rear of the rotor disk due to downward front wake convection with longitudinal distance. A lateral tilt of the front rotor wake towards its advancing side, as it convects downstream, results in the advancing tip of the aft rotor operating in the upwash of the front rotor's retreating side rollup vortex.

2. When compared to an isolated rotor in edgewise flight, the aft rotor of a two rotor system is observed to produce less thrust and require greater torque, with the loss predominantly at the front of the rotor disk. In particular, an aft rotor $2.5R$ behind, and vertically aligned with the front rotor is observed to produce 8.4% less thrust than an isolated rotor and require 13.4% higher torque.

3. As vertical rotor spacing increases, and the distance between the aft rotor and the front rotor's wake grows larger, the downwash observed by the aft rotor reduces. The reduction in downwash causes the loss in lift compared to an isolated rotor to reduce. Similarly, the torque penalty on the aft rotor decreases with vertical separation. For an aft rotor spaced $2.5R$ behind the front rotor, a $0.5R$ vertical offset reduces the lift deficit to 4.6% and the torque penalty to 6.8%.

4. As longitudinal spacing is increases, the downwash observed by the aft rotor again decreases. Increased longitudinal separation allows the front rotor wake to convect down farther by the time it reaches the aft rotor. The reduction in downwash causes the aft rotor lift deficit and torque penalty to decrease in magnitude. The improvements in lift and torque going from $2.5R$ to $3R$ longitudinal separation are modest, but larger improvements are seen going from $3R$ to $3.5R$. A rotor at $3.5R$ longitudinal separation (and zero vertical offset) shows a 5.8% lift deficit and 10.4% torque penalty.

5. Over the range of parameters considered in this study, vertical separation was more effective in minimizing interactional aerodynamic effects. Compared to an aft rotor $2.5R$ behind the front rotor and with zero vertical offset exhibiting a lift deficit of 8.4%, increasing its vertical offset to $0.5R$ (same longitudinal separation of $2.5R$) reduced the lift deficit to 4.6%. In contrast, increasing the longitudinal offset to $3.5R$ (keeping zero vertical separation) reduced the lift deficit to 5.8%. Similarly, compared to the 13.4% torque penalty for a rotor $2.5R$ aft and in-plane with the front rotor, increasing its vertical offset to $0.5R$ (same longitudinal position) decreases the torque penalty to 6.8%. In contrast, increasing the longitudinal offset to $3.5R$ (keeping zero vertical separation) decreases the torque penalty to 10.4%. With a $0.5R$ vertical offset of the aft rotor, further increase in longitudinal offset (above $2.5R$) produces limited benefits.

REFERENCES

[1]S. Yoon, T. H. Pulliam, and N. M. Chaderjian, "Simulations of XV-15 Rotor Flows in Hover Using OVERFLOW," in *AHS 5th Aeromechanics Specialists Conference, San Francisco, CA, USA*, Jan 2014.

[2]S. Yoon, H. C. Lee, and T. H. Pulliam, "Computational Analysis of Multi-Rotor Flows," in *AIAA 54th Aerospace Sciences Meeting, San Diego, CA, USA*, Jan. 2016.

[3]S. Yoon, P. V. Diaz, D. D. Boyd Jr., W. M. Chan, and C. R. Theodore, "Computational aerodynamic modeling of small quadcopter vehicles," in *Proceedings of the 73rd Annual Forum*, (Fort Worth), AHS International, May 2017.

[4]Y. Tanabe, "Numerical Simulations of Aerodynamic Interactions Between Multiple Rotors," in *42nd European Rotorcraft Forum*, 2016.

[5]P. Ventura Diaz and S. Yoon, "High-Fidelity Computational Aerodynamics of Multi-Rotor Unmanned Aerial Vehicles," No. 0 in AIAA SciTech Forum, American Institute of Aeronautics and Astronautics, Oct. 2018.

[6]P. V. Diaz, S. Yoon, and C. R. Theodore, "High-fidelity computational aerodynamics of the elytron 4s uav," in *AHS Specialists Meeting - Aeromechanics, San Francisco, CA, USA*, Jan. 2018.

[7]M. Misiorowski, F. Gandhi, and A. A. Oberai, "A computational study on rotor interactional effects for a quadcopter in edgewise flight," in *Proceedings of the 74th Annual Forum*, (Phoenix), AHS International, May 2018.

[8]Whirlwind Propellers, "https://whirlwindpropellers.com/airboats/shop/razor-x/," 2018.

[9]F. G. Robert Niemiec, "Development and Validation of the Rensselaer Multicopter Analysis Code (RMAC): A Physics-Based Low-Fidelity Modeling Tool," in *75th Annual Forum of the Vertical FLight Society*, (Philadelphi), 2019.

[10]F. Giannini, A. Kaufman, and M. Kearney, "Configuration development and subscale flight testing of an urban mobility evtol," in *Aeromechanics Design for Transformative Vertical Flight*, (San Francisco), AHS International, January 2018.

[11]K. E. Jansen, C. H. Whiting, and G. M. Hulbert, "A generalized-alpha method for integrating the filtered navier-stokes equations with a stabilized finite element method," 2000.

[12]A. N. Brooks and T. J.R. Hughes, "Streamline Upwind/Petrov-Galerkin Formulations for Convection Dominated Flows with Particular Emphasis on the Incompressible Navier-Stokes Equations," *Computer Methods in Applied Mechanics and Engineering*, vol. 32, pp. 199–259, 09 1982.

[13]R. Niemiec and F. Gandhi, "Effects of Inflow Model on Simulated Aeromechanics of a Quadrotor Helicopter," in *AHS International 72nd Annual Forum and Technology Display*, (West Palm Beach, FL, USA), May 2016.